A LATTICE-GAS CELLULAR AUTOMATON MODEL FOR IN VITRO SPROUTING ANGIOGENESIS*

C. Mente[a†], I. Prade[b], L. Brusch[a], G. Breier[b], A. Deutsch[a]

[a]Center for Information Services and High Performance Computing
Dept. for Innovative Methods of Computing, Technische Universität Dresden
Nöthnitzer Strasse 46, 01062 Dresden, Germany
[b]Institute of Pathology, Universitätsklinikum Carl Gustav Carus
Technische Universität Dresden
Schubertstrasse 15, 01307 Dresden, Germany

(Received December 20, 2011)

The mechanisms of sprout formation and branching during sprouting angiogenesis are only partially understood and mostly attributed to nonlocal signals mediated by the heterogeneous distribution of vascular endothelial growth factor (VEGF). Here, we show that purely local mechanisms can account for angiogenic network formation. In particular, we examine the effects of homogeneous stimulation by VEGF on local endothelial cell–cell interactions and on interactions between endothelial cells and the microenvironment. We adopt a cell-based mathematical modeling approach (lattice-gas cellular automaton) and fit our model to image data obtained from *in vitro* experiments tailored to homogeneous conditions. This approach reveals the basal effects of (homogeneous) VEGF stimulation, in particular increased movement coordination and cell–cell adhesion but no significant change in contact guidance and extracellular matrix remodeling.

DOI:10.5506/APhysPolBSupp.5.99
PACS numbers: 87.10.Hk, 87.10.Mn, 87.18.Hf

1. Introduction

Angiogenesis is the process of novel blood vessel formation by sprouting. During angiogenesis sprouts of endothelial cells grow from existing vessels in response to biochemical signals. Angiogenic sprouting is traditionally subdivided into different phases [1]. First, endothelial cells locally degrade the basement membrane (composed of extracellular matrix ingredients), through the activity of proteases. Second, under the influence of VEGF, an endothelial cell adopts the tip cell phenotype and migrates into the surrounding

* Presented at the Summer Solstice 2011 International Conference on Discrete Models of Complex Systems, Turku, Finland, June 6–10, 2011.

† Corresponding e-mail address: carsten.mente@tu-dresden.de

tissue. Stalk cells that are attached to the tip cell follow and proliferate, leading to the extension of the vascular sprout. Third, the growing sprout forms a lumen. In the living organism, perivascular cells are recruited to the newly formed blood vessel leading to its maturation and stabilization. Angiogenesis plays a key role during wound healing and different pathological processes, *e.g.* tumor formation, inflammation and ocular diseases [2, 3, 4]. Unraveling the precise biological mechanisms governing angiogenesis, can lead to improved treatments by helping to identify potential drug targets.

A multitude of mechanisms is active during angiogenesis, including intercellular adhesion, contact guidance, extra-cellular matrix remodeling and inter-cellular movement coordination [2, 3, 4, 5, 6, 7, 8, 9, 10, 11]. The prevailing hypothesis is that angiogenic sprouting is regulated through contact-inhibited chemotaxis in combination with VEGF gradients [6, 8, 12, 13, 14], *i.e.* angiogenic sprouting arises due to long-range interactions. However, *in vitro* assays excluding long-range interactions also exhibit angiogenic sprouting [1]. There one observes that direct cell–cell and cell-environment interactions, especially interactions between endothelial cells and the extracellular matrix, can also drive angiogenic sprouting under homogeneous VEGF administration. However, the precise regulation of sprouting on the basis of local mechanisms is still not understood.

Here, we examine the effects of homogeneous VEGF on local interactions of endothelial cells during early *in vitro* angiogenesis with a mathematical model. These effects are reflected in the parameter values of four cellular interactions. We apply a gradient-based parameter estimation technique [15] and fit the model to image data obtained from *in vitro* experiments. In [15] *in vitro* angiogenic sprouting was only used for demonstration of the parameter estimation technique without regard for specific biological questions. In this article, we focus instead on applying the parameter estimation technique to answer the specific biological question stated above, the effects of homogeneous VEGF on local interactions of endothelial cells. We utilize image data from two different sets of *in vitro* experiments: with and without additional homogeneous VEGF administration. In particular, the number and lengths of developing sprouts, and the radius of the evolving pattern are compared in simulations and experiments.

The article is structured as follows. First, we describe the setup of the *in vitro* experiments which provide the experimental image data. Next, we introduce the mathematical model, address the scaling of the model and define the observables used for parameter estimation. We then study the influence of VEGF on the interplay of cell interactions during angiogenesis *in vitro* sprouting assays. Finally, we discuss the biological interpretation of our results.

2. In vitro experiments

Dextran-coated Cytodex 3 microcarriers (Amersham Pharmacia Biotech, Piscataway, NJ) were coated with human umbilical vascular endothelial cells (HUVEC; Lonza, Cologne) essentially as described by [1]. Beads were embedded in fibrin gel in 96-well plates consisting of 2.5 mg/ml of fibrinogen (Sigma, Steinheim, Germany), 0.1 units/ml of aprotinin (Sigma) and EGM-2 (with 2% FCS). Clotting of fibrinogen was induced by adding 8 μl of 10 U/ml thrombin (Sigma) per well. Five thousand human skin fibroblasts Detroit 551 (Promocell, Heidelberg, Germany) were plated on top of the fibrin gel to provide growth factors necessary for endothelial cell growth and survival. Cultures were incubated at 37°C in atmosphere containing 5% CO_2, 21% O_2, and were monitored for a maximum of 3 days. Medium was changed every other day. Experiments were performed in regular endothelial growth medium (EGM-2 with 2% FCS) with or without addition of 1 μl recombinant VEGF (2 μg/ml; Lonza). Two independent experiments were performed under the same conditions (Table I). Experimental image data were obtained by bright-field microscopy after 48 or 72 hours, respectively. Sprouts growing away from the bead are shown in Fig. 1 (a). The following parameters

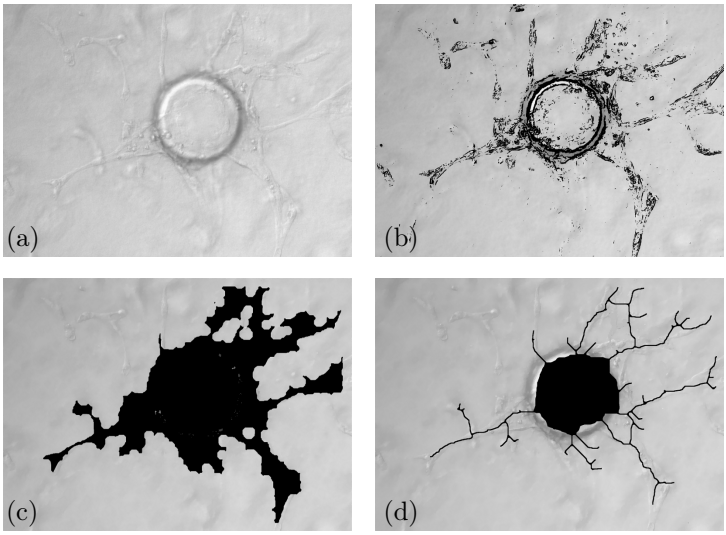

Fig. 1. Automatic extraction of observables from experimental images. Application of the automatic process to an example image; (a)–(d) show the subsequent image processing steps, the observables are then calculated from image (d). (a) Original, experimental image, (b) smoothing with an anisotropic diffusion filter and edge detection with the Sobel operator, (c) morphological closing and opening, removal of disconnected parts, (d) morphological thinning.

were determined: cumulative length of all sprouts, number of sprouts, and maximum distance between the center of the bead and the tip of the longest sprout. We obtained 25 different data sets (*i.e.* data from 25 different beads) from experiment 1, and 10 data sets from experiment 2.

TABLE I

Time and number of data sets for both experiments.

	Time in h	Number of data sets
Experiment 1	48	25
Experiment 2	72	10

3. Mathematical model

We employ a LGCA (lattice-gas cellular automaton) model [16,17,18,19, 20,21] to represent the interactions of endothelial cells with each other and the (artificial) extra-cellular matrix in the *in vitro* assay (see Sec. 2). This approach excludes a detailed description of the actual biological realization of cell interactions. Instead we focus solely on their effect on endothelial cells and the extra-cellular matrix. Here, this abstract description is sufficient, since the purpose of our mathematical model is to study the influence of VEGF on the effects of cell interactions and not on the specific details of underlying molecular mechanisms.

Specifically, we adopt the lattice-gas cellular automaton model from [15]. In our model, the extra-cellular matrix is considered as an additional lattice with states that represent the local orientation of ECM-fibers. In the model we are treating the results of extra-cellular matrix dissolution and reassembly as changes in the local orientation of ECM-fibers. An overview of respective mechanisms and parameters considered in the mathematical model is presented in Table II.

The experimental *in vitro* assay is very thin compared to its length and width (height 0.5 mm, width 5 mm and length 5 mm) and the observed patterns (see previous section) are two-dimensional. A two-dimensional model is therefore a sufficient approximation. Initial conditions define a fully occupied circular area with a radius of 5 nodes at the center of the lattice. In each time step every node in this area is refilled to mimic the experimental conditions (a reservoir of cells at the bead in the center of the gel).

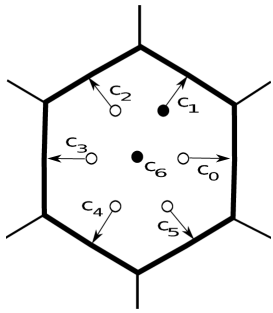

Fig. 2. Node of hexagonal two-dimensional lattice (example). There are six velocity channels $c_0, c_1, c_2, c_3, c_4, c_5$ and one rest channel c_6, respectively. Filled circles denote occupied channels.

Here, we use a LGCA with two-dimensional hexagonal lattice $\mathcal{L}$ with six velocity channels:

$$c_0 := (1,0)^T, \qquad c_1 := \left(\frac{1}{2}, \frac{\sqrt{3}}{2}\right)^T, \qquad c_2 := \left(-\frac{1}{2}, \frac{\sqrt{3}}{2}\right)^T,$$

$$c_3 := (-1,0)^T, \qquad c_4 := \left(-\frac{1}{2}, -\frac{\sqrt{3}}{2}\right)^T, \qquad c_4 := \left(\frac{1}{2}, -\frac{\sqrt{3}}{2}\right)^T,$$

and one rest channel $c_6 := (0,0)^T$. In the model, endothelial cells are described by states $\eta(r) = (\eta_0(r), \ldots, \eta_6(r)) \in \mathcal{E} = \{0,1\}^7$ at lattice nodes $r \in \mathcal{L}$.

The transition rule in a LGCA model consists of two subsequent steps: an interaction and a migration step. Interactions are specified by probability distributions $P(\eta_{\mathcal{N}_r} \to \eta')$ with $\eta' \in \mathcal{E}$, and $\eta_{\mathcal{N}_r} \in \mathcal{E}^7$ giving the configuration at r and in the next-neighbor neighborhood $\mathcal{N}_r := \{r + c_i |\ i = 0, \ldots, 5\}$. In the following, we define the mechanisms (see Table II) included in the model, namely cell–cell **adhesion**, **movement coordination** of endothelial cells, **contact guidance** along the extracellular matrix and **remodeling** of the extra-cellular matrix by endothelial cells [4, 22, 23].

Endothelial cells *in vitro* "stick" to each other by cell adhesion. In the mathematical model we describe this interaction by a mechanism which gives cells a preference to stay in the neighborhood of other cells, *i.e.* choosing their movement direction $J(\eta') := \sum_{i=0}^{5} \eta'_i c_i$, depending on $\rho_{\mathcal{N}_r} := \sum_{i=0}^{5} \sum_{j=0}^{6} \eta_j(r + c_i) c_i$, which gives the directions towards the highest number of cells in the neighborhood (illustrated in Fig. 3 (a))

$$P_{\mathrm{ad}}\left(\eta_{\mathcal{N}_r} \to \eta'\right) = \frac{\exp\left(\beta_{\mathrm{ad}} \left\langle \rho_{\mathcal{N}_r}, J\left(\eta'\right)\right\rangle\right)}{Z_{\mathrm{ad}}},$$

TABLE II

Overview of model mechanisms and parameters.

Mechanism	Model realization	Parameter
Adhesion	Flux toward higher concentration of cells	β_{ad}
Movement coordination	Flux parallel to the flux of the neighbors	β_{mov}
Contact guidance	Flux parallel to ECM-orientation	β_{con}
Remodeling	ECM-reorientation parallel to cell flux	β_{rem}

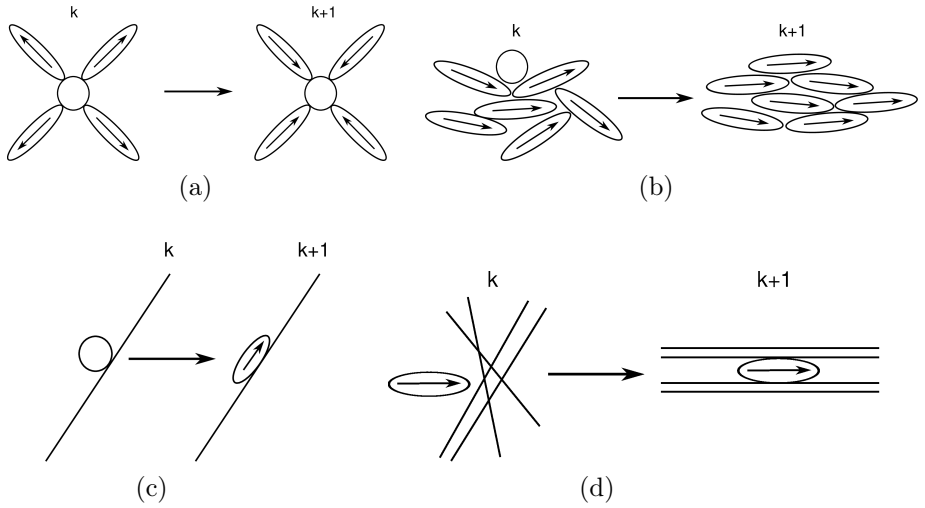

Fig. 3. Illustration of model mechanisms. Effects of adhesion (a), movement coordination (b), contact guidance (c) and ECM remodeling (d) during one time step. Circles indicate endothelial cells at rest. Moving endothelial cells are indicated by ovals; arrows indicate the direction of motion. Straight lines indicate extra-cellular matrix fibers.

the parameter $\beta_{\text{ad}} \in \mathbb{R}$ controls the adhesivity in the model and Z_{ad} is a normalization term. During angiogenesis endothelial cells move collectively. This is reflected in the model by synchronizing the cells' movement directions $J(\eta')$ with their neighbors' $J_{\mathcal{N}_r} := \sum_{i=0}^{5} \sum_{j=0}^{6} \eta_j(r+c_i)c_j$. We call this

mechanism movement coordination (Fig. 3 (b)). It is controlled by the parameter β_{mov} and the corresponding transition probability $P_{\text{mov}}(\eta_{\mathcal{N}_r} \to \eta')$ is given by

$$P_{\text{mov}}\left(\eta_{\mathcal{N}_r} \to \eta'\right) = \frac{\exp\left(\beta_{\text{mov}} \left\langle J_{\mathcal{N}_r}, J(\eta')\right\rangle\right)}{Z_{\text{mov}}},$$

Z_{mov} is a normalization term. Beside cell–cell interactions we model interactions between endothelial cells and the extra-cellular matrix, contact guidance and remodeling. Here, the extra-cellular matrix is considered as an additional lattice with $\theta \in [0, \pi]$ at every node. The spatial orientation of the extra-cellular matrix at node r is given by $E(\theta(r)) := (\cos(\theta), \sin(\theta))^T$. Endothelial cells are guided by the extra-cellular matrix by contact guidance. In the model contact guidance tries to synchronize the direction of movement of the cells $J(\eta')$ with the spatial orientation $E(\theta(r))$ of the extra-cellular matrix (Fig. 3 (c)) and is described by the corresponding transition probability controlled by the parameter β_{con}

$$P_{\text{con}}\left(\eta_{\mathcal{N}_r} \to \eta'\right) = \frac{\exp\left(\beta_{\text{con}} \left|\left\langle E\left(\theta(r)\right), J\left(\eta'\right)\right\rangle\right|\right)}{Z_{\text{con}}},$$

Z_{con} is a normalization term. Endothelial cells remodel the extra-cellular matrix by aligning it parallel to their direction when they move through it. In the model, remodeling of the extra-cellular matrix is controlled by the parameter β_{rem}, which tries to synchronize the spatial orientation $E(\theta'(r))$ of the extra-cellular matrix with the movement direction $J(\eta(r))$ of the cells (Fig. 3 (d))

$$P_{\text{rem}}(\theta(r) \to \theta'(r)) = \frac{\exp\left(\beta_{\text{rem}} \left\langle E\left(\theta'\right), J(\eta(r))\right\rangle\right)}{Y}, \tag{1}$$

Y is a normalization term. The interactions P_{ad}, P_{mov} and P_{con} are independent from each other per construction. Hence we can combine them by multiplication to obtain the interaction probability $P(\eta_{\mathcal{N}_r} \to \eta')$:

$$P\left(\eta_{\mathcal{N}_r} \to \eta'\right) = P_{\text{ad}}\left(\eta_{\mathcal{N}_r} \to \eta'\right) P_{\text{mov}}\left(\eta_{\mathcal{N}_r} \to \eta'\right) P_{\text{con}}\left(\eta_{\mathcal{N}_r} \to \eta'\right). \tag{2}$$

Then, the interaction step consists of the application of both $P(\eta_{\mathcal{N}_r} \to \eta')$, which depends on the parameters β_{ad}, β_{mov} and β_{con}, and $P_{\text{rem}}(\theta(r) \to \theta'(r))$, which depends on β_{rem} to obtain new states $\eta'(r)$ and $\theta'(r)$ for all nodes r. The migration step is only applied to the cells (ECM fibers do not migrate in the model). The new states $\eta''(r)$ after migration are given by

$$\eta_i''(r) := \eta_i'(r - c_i), \qquad i = 0, \ldots, 6$$

for all nodes $r \in \mathcal{L}$.

Scaling: One node in the model is defined as 15μm in diameter. For the first experiment, image data was obtained after 48 hours and for the second experiment after 72 hours, respectively. Based on the image data, we estimate that endothelial cells move with an average speed of $\approx 7\mu$m or 0.5 nodes per hour. Accordingly, one time step in the model corresponds to 2 hours in the experiment.

4. Data analysis

Since we want to quantitatively compare experiments with simulations we need to introduce observables which can be measured in both. Here we use the following observables: summed sprout length, average sprout number and average pattern radius. A sprout is defined as a chain of cells, see Fig. 1. Values of experimental observables are automatically obtained from experimental images (see Fig. 1). Parameters in the LGCA model are calibrated to match these observables with the parameter estimation algorithm developed in [15], which finds globally optimal parameters in LGCAs by a two-phase optimization algorithm. In the first phase, local optima are identified through gradient-based optimization using Algorithmic differentiation to calculate the necessary gradient information. In the second phase, a multi-level single-linkage method is used for global optimization of the parameter set. In this parameter estimation algorithm, the experimental observables are used as constants and we can directly use the values we automatically measured from experiments. However, to apply the cited parameter estimation algorithm, a functional description in the form of simple functions (here this means addition and multiplication) of the observables measured from simulations is necessary. In the following, we construct this functional description for our observables based on geometric moments [24, 25, 26]. Let $I(x, y)$ be a binary image of dimension $n \times m$ $(n, m \in \mathbb{N}, x \in [0, \ldots, n-1], y \in [0, \ldots, m-1])$.We can a obtain a binary images from the two-dimensional LGCA model introduced in the previous section by setting

$$I(x,y) = \begin{cases} 1 & \text{if} \quad \sum_{i=0}^{6} \eta_i(r) > 0 \\ 0 & \text{if} \qquad\qquad \text{else} \end{cases} .$$

With $r := A^{-1}(x, y)^T$, A^{-1} gives the coordinates transformation between the image and the hexagonal lattice and has the form

$$A^{-1} = \frac{1}{2} \begin{pmatrix} 2 & -1 \\ 0 & \sqrt{3} \end{pmatrix} .$$

The **geometric moment** m_{pq} of the order of p-q with $p, q \in \mathbb{N}$ is defined as

$$m_{pq} = \sum_{x=0}^{n-1} \sum_{y=0}^{m-1} x^p y^q I(x,y) \,.$$

Similarly, the translation-invariant **central geometric moment** μ_{pq} is defined as

$$\mu_{pq} = \sum_{x=0}^{n-1} \sum_{y=0}^{m-1} (x-\bar{x})^p (y-\bar{y})^q I(x,y) \,,$$

with

$$\bar{x} = \frac{m_{10}}{m_{00}} \,, \qquad \bar{y} = \frac{m_{01}}{m_{00}} \,.$$

These geometric moments do not contain information about spatial correlations between neighboring nodes. However, such information is required for detecting sprouts. Therefore, we modify the geometric moments as

$$\mu'_{pq,M} = \sum_{x=0}^{n-1} \sum_{y=0}^{m-1} (x-\bar{x})^p \, (y-\bar{y})^q \, N_M(x,y) \,,$$

$$N_M(x,y) := \prod_{(x',y') \in \mathcal{N}(x,y)} I\left(x',y'\right)^{M(x'-x,y'-y)} \left(1 - I(x',y')\right)^{(1-M(x'-x,y'-y))} \,,$$

where $\mathcal{N}(x,y) = \{(x,y) + (x',y') | (x',y') \in \bar{\mathcal{N}}\}$ and

$$\bar{\mathcal{N}} := \{(0,0),(1,0),(1,1),(0,1),(-1,0),(-1,-1),(0,-1)\} \,.$$

Furthermore, the binary mask $M(x,y)$ specifies the desired neighborhood configurations. Only sites (x,y) for which neighborhood $I(x',y')$ is equal to $M(x'-x,y'-y)$ for all $(x',y') \in \mathcal{N}(x,y)$ contribute to $N_M(x,y)$. In the following, we define sprouts as chains of connected cells, and construct our observables summed sprout length and number of sprouts based on the modified moments of the order of 0-0. The idea is essentially to count all nodes with a predefined amount of occupied neighbors. In the following, we express binary masks M by ordered tuples $\bar{M} = \{M_0, \ldots, M_6\}$ with the following relation between them

$$M(x,y) = \begin{cases} \bar{M}_0 & \text{if } (x,y) = (0,0) \\ \bar{M}_1 & \text{if } (x,y) = (1,0) \\ \bar{M}_2 & \text{if } (x,y) = (1,1) \\ \bar{M}_3 & \text{if } (x,y) = (0,1) \\ \bar{M}_4 & \text{if } (x,y) = (-1,0) \\ \bar{M}_5 & \text{if } (x,y) = (-1,-1) \\ \bar{M}_6 & \text{if } (x,y) = (0,-1) \end{cases} .$$

Thus, on a hexagonal lattice, the summed sprout length, which is the sum of the individual lengths of each sprout, l_{sprouts}, is given by

$$l_{\text{sprouts}} = \sum_{M^j} \mu'_{00,M^j} ,$$

with $\bar{M}^j$, $j = 0, \ldots, 5$:

$$\begin{aligned} &\bar{M}^0 = (1,1,0,0,1,0,0), \quad \bar{M}^1 = (1,0,1,0,0,1,0), \quad \bar{M}^2 = (1,0,0,1,0,0,1), \\ &\bar{M}^3 = (1,1,1,0,0,0,0), \quad \bar{M}^4 = (1,0,1,1,0,0,0), \quad \bar{M}^5 = (1,0,0,1,1,0,0), \\ &\bar{M}^6 = (1,0,0,0,1,1,0), \quad \bar{M}^7 = (1,0,0,0,0,1,1), \quad \bar{M}^8 = (1,1,0,0,0,0,1), \\ &\bar{M}^9 = (1,1,0,1,0,0,0), \quad \bar{M}^{10} = (1,0,1,0,1,0,0), \quad \bar{M}^{11} = (1,0,0,1,0,1,0), \\ &\bar{M}^{12} = (1,0,0,0,1,0,1), \quad \bar{M}^{13} = (1,1,0,0,0,1,0), \quad \bar{M}^{14} = (1,0,1,0,0,0,1). \end{aligned}$$

Here, a node is counted as part of a sprout if it is occupied (there is at least one cell at the node) and has exactly two occupied neighbors. The sum over all such nodes determines the total length of all sprouts. Note, that sprout branching points are not counted as part of sprouts. The number of sprouts (= number of tips) n_{sprouts} is

$$n_{\text{sprouts}} = \sum_{M^j} \mu'_{00,M^j} ,$$

with $\bar{M}^j$, $j = 0, \ldots, 5$:

$$\begin{aligned} &\bar{M}^0 = (1,1,0,0,0,0,0), \ \bar{M}^1 = (1,0,1,0,0,0,0), \ \bar{M}^2 = (1,0,0,1,0,0,0), \\ &\bar{M}^3 = (1,0,0,0,1,0,0), \ \bar{M}^4 = (1,0,0,0,0,1,0), \ \bar{M}^5 = (1,0,0,0,0,0,1). \end{aligned}$$

Here, a node is counted as a tip if it is occupied and has exactly one occupied neighbor. The sum over all these nodes determines the number of sprouts.

For the calculation of the total sprout length and the sprout number only occupied nodes which are connected to the bead are considered, *i.e.* detached cells are not counted. Additionally, we define an observable called pattern radius which is the maximum distance between the center of the bead and any tip. We define the squared error $F(\beta)$

$$F(\beta) = \sum_{i=0}^{2} w_i (f_i(\beta) - g_i)^2 \,, \tag{3}$$

with the simulation observables f_i, experimental observables g_i, weights w_i and the parameters $\beta = (\beta_{\mathrm{ad}}, \beta_{\mathrm{mov}}, \beta_{\mathrm{con}}, \beta_{\mathrm{rem}})$. The observables are the summed sprout length ($i = 0$), the number of sprouts ($i = 1$) and the pattern radius ($i = 2$). We characterize the change of the squared error $F(\beta)$ under parameter changes around a local minimum β with the quadratic function $F_{\mathrm{quad}}(\tilde{\beta}_i)$ defined by

$$F_{\mathrm{quad}}\left(\tilde{\beta}_i\right) = \frac{\left(\tilde{\beta}_i - \beta_i\right)^2}{F(\beta)} \frac{\partial F(\beta)}{\partial \beta_i} \,, \tag{4}$$

with $\beta = (\beta_{\mathrm{ad}}, \beta_{\mathrm{mov}}, \beta_{\mathrm{con}}, \beta_{\mathrm{rem}})$ and $\tilde{\beta}_i, \beta_i \in (\beta_{\mathrm{ad}}, \beta_{\mathrm{mov}}, \beta_{\mathrm{con}}, \beta_{\mathrm{rem}})$.

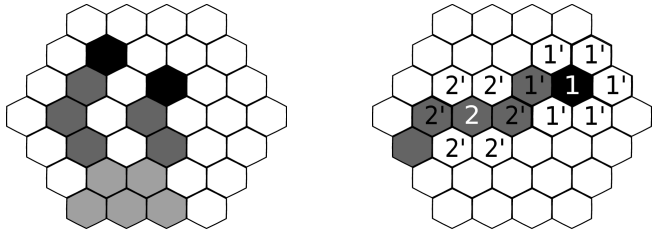

(a) (b)

Fig. 4. Example: node types. Sub-figure (a) shows the four different node types that can occur. There are two types of occupied nodes used to calculate the observables: tip nodes (black) and sprout nodes (dark gray). In addition, there are occupied nodes that are neither sprout nor tip nodes (light gray) and empty nodes (white). Sub-figure (b) illustrates two nodes marked as 1 and 2, and their neighborhoods $1'$ and $2'$, respectively. Node 1 is a tip node because there is only one occupied node in its neighborhood while node 2 is sprout node because there are exactly two occupied nodes in its neighborhood.

5. Results and discussion

We have modeled the early phase of *in vitro* sprouting angiogenesis under homogeneous VEGF stimulation and quantitatively compared experiments and simulations. Our model contains no long-range interactions, only local

interactions of endothelial cells with each other and with their microenvironment are considered. Fig. 5 shows simulation patterns for control and VEGF group, respectively. The development of distinct sprouts can be observed in both cases. In the VEGF case, length and number of sprouts are larger than in the control group. In Fig. 6 the values of the observables, number of sprouts, summed sprout length and pattern radius, are compared between experiment and simulation for the control group and VEGF. Suitable parameter sets for simulations were obtained by a recently developed parameter estimation method [15]. Simulation results were obtained by averaging over 500 simulation runs with the same parameter sets. The experimental data was obtained by averaging over 25 data sets (experiment 1) and over 10 data sets (experiment 2), respectively.

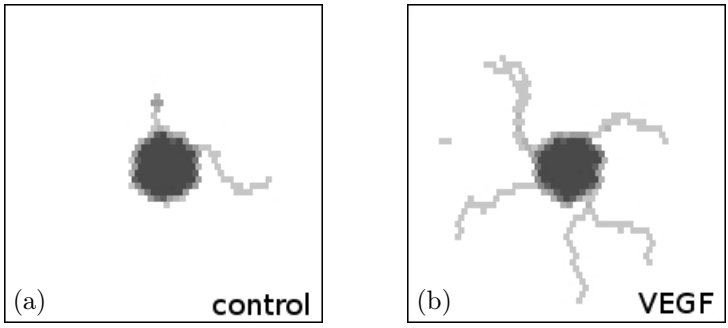

Fig. 5. Simulations for the control group and VEGF stimulation. Simulations use the parameter values obtained with parameter estimation [15]. We show simulations for the control group (a) and VEGF stimulation (b). Nodes containing endothelial cells are shown grey, the intensity indicates cell density. Empty nodes are shown in white. The bead in the center is displayed in dark grey. Note, that for the majority of sprout nodes only one channel is occupied.

In both experiments, there is a good agreement between the values of observables (summed sprout length, average sprout number and average pattern radius) of the simulation the experimental data for the control and the VEGF groups. In experiment 2 all three observables show no significant difference between experiment and simulation. In experiment 1, there is no significant difference for the values of the summed sprout length in the control and VEGF group, while for the other two observables there is either no significant difference or only slight underestimation of the values.

Fig. 7 exhibits the effect of VEGF on the model parameters, *i.e.* on the strength of the different cell interactions. It can be observed that in experiment 1 VEGF increases the movement coordination parameter by $\approx 25\%$ compared to the control group and the cell adhesion parameter by $\approx 10\%$ (Fig. 7 (a), (b)). In experiment 2, VEGF increases the movement coordi-

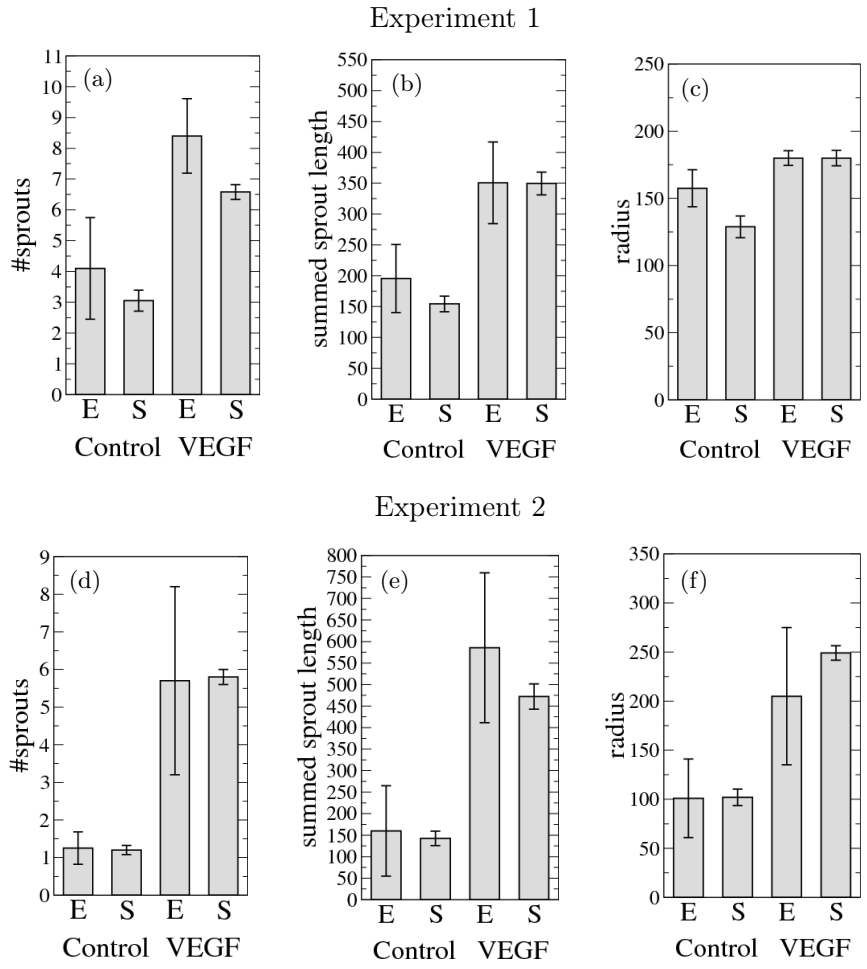

Fig. 6. Comparison of *in vitro* experiments (E) and simulations (S). Simulations use the parameter values obtained with parameter estimation [15]. Figures (a)–(c) show comparisons with data from experiment 1 and figures (d)–(f) with experiment 2. Simulation results are obtained by averaging over 500 simulation runs with the same parameter sets; the error bars indicate the standard error within a 99% confidence interval. Experimental data was obtained by averaging over 25 data sets (experiment 1) and over 10 data sets (experiment 2), respectively; error bars represent the standard deviation. Averaged summed sprout lengths and averaged radii are given in μm.

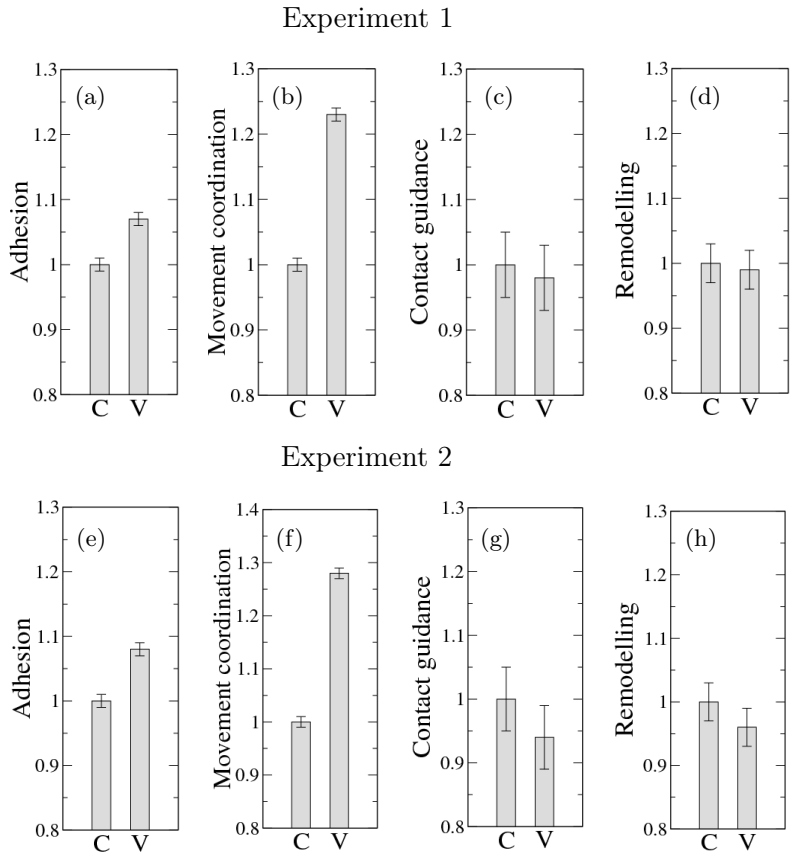

Fig. 7. Comparison of the control group (C) and VEGF (V). The parameter values for cell adhesion were obtained with parameter estimation [15] and normalized such that the adhesion parameter value for the control group equals 1. Number of sprouts, summed sprout length and pattern radius were used for parameter optimization. Bars are the parameter ranges of $\beta_i \in (\beta_{\text{ad}}, \beta_{\text{mov}}, \beta_{\text{con}}, \beta_{\text{rem}})$ for which $F_{\text{quad}}(\beta_i) \leq 1$ with $F_{\text{quad}}(\beta_i)$ defined by (4). Short bars indicate parameters with high sensitivity to changes while large bars indicate those with low sensitivity. Figures (a)–(d) show results for experiment 1 and figures (e)–(h) for experiment 2, respectively. In the VEGF case an increase of $\approx 10\%$ in cell adhesion (a) and of $\approx 25\%$ in movement coordination (b) can be observed in experiment 1. In experiment 2, one observes an increase of $\approx 8\%$ in cell adhesion (e) and of $\approx 27.5\%$ in movement coordination (f) if VEGF is added. Only a slight, inconclusive decrease in contact guidance and remodeling can be observed in both experiments (c), (d), (g), (h).

nation parameter by $\approx 25\%$ and the cell adhesion parameter by $\approx 8\%$ (Fig. 7 (e), (f)). In both experiments only an insignificant change in the parameters corresponding to contact guidance of endothelial cells and remodeling of the extracellular matrix is observed (Fig. 7 (c), (d), (g), (h)). Therefore, the influence of VEGF on contact guidance of endothelial cells and on remodeling of the extra-cellular matrix appears to be negligible. Furthermore, Fig. 7 reveals that our model is more sensitive to changes in the adhesion and movement coordination parameters compared to changes in parameters corresponding to contact guidance and remodeling. This additionally supports the argument that in our model VEGF mainly influences adhesion and movement coordination.

In summary, we have demonstrated that including only local cell interactions in our model can quantitatively reproduce experimental data. Local interactions are therefore sufficient for angiogenic network formation *in vitro* sprouting assays, *i.e.* no additional non-local mechanisms, *e.g.* VEGF gradients, are required.

Our results reveal the effect of VEGF on the interplay of cell interactions during angiogenesis *in vitro* sprouting assays. These effects were consistently found in two independent series of experiments. From the model we infer an increase in cell adhesion when VEGF is added. Cell adhesion in endothelial cells is mediated primarily due to adhesive junctions by VE-cadherin [27]. Therefore, in our model there is an increase in the activity of adhesive junctions, *i.e.* an increase in the activity of VE-cadherin. VEGF is known to stimulate the production of proteases in endothelial cells, stimulate their migration and proliferation, and loosen cell–cell contacts though modification of VE-Cadherin [28, 29, 30]. Our results appear to be partially inconsistent with these known responses to VEGF. It is important to note, however, that some of the VEGF effects, notably protease production and loosening of cell–cell contacts, relate only to the initiation of vascular sprouting, but not to the extension and branching of the growing sprout. Stalk cells need to adhere tightly to the tip cell, and to each other, and they do so in the presence of VEGF. This important aspect has not been appreciated in the literature so far. Whether VEGF exerts this effect directly or indirectly, via other endothelial signaling pathways, remains to be investigated. It has been shown that VEGF induces Notch-Delta signaling, leading to the repression of the tip cell phenotype in stalk cells [8]. It is possible that this pathway also contributes to the increased cell adhesion that we observe in our model. From our model we can also infer an increase of movement coordination when VEGF is added. Besides cell–cell adhesion, movement coordination also requires coordinated cytoskeletal activity for joint force generation. The coordination of cell movement vectors, *i.e.* cell alignment, is likely communicated by paracrine signaling [23]. Accordingly, the increase

of movement coordination under VEGF in our model suggests an increase in the concentration of paracrine signaling molecules under VEGF in the *in vitro* assay. However, the exact biological mechanisms of super-cellular cytoskeletal organization have not been determined so far [23]. In our model there is no change in the strength of contact guidance when VEGF is added. Contact guidance of endothelial cells by the extracellular matrix is mediated by integrins [9]. Experimental findings suggest that VEGF promotes the expression of integrins in activated endothelial cells compared to quiescent endothelial cells [31]. This is no contradiction to our result since we have considered only activated endothelial cells. Seen in this light, we interpret our results to show that additional VEGF does not further increase the expression of integrin in already activated endothelial cells. From the model we also cannot deduce any change in the magnitude of extra-cellular matrix remodeling. Remodeling of the extra-cellular matrix by endothelial cells is mediated by metalloproteinases [10, 11]. Thus, according to our model there is no significant change in metalloproteinases activity due to VEGF. This corresponds to the already known fact that VEGF does not induce the expression of members of the proteases family except collagenase. Furthermore, significant expression of collagenase occurs only at higher concentrations of VEGF [30, 32].

In future work, we are going to use the existing model to study the early phase of *in vitro* angiogenesis under different experimental conditions, in particular hypoxia. Furthermore, experimental data from later stages of *in vitro* angiogenesis and from in vivo experiments will be considered. An interesting question is if local cell–cell interactions are also sufficient to explain later stages of angiogenesis. To address this question the model will be extended accordingly, *i.e.* lumen formation, cell signaling, space and time-dependent concentrations of growth factors, and the effects of blood flow on the developing vessels are going to be explicitly included.

We are grateful to Walter de Back (Dresden) for fruitful discussions. We acknowledge support by the German Ministry for Education and Research (BMBF) through grants no. 0315259 and no. 0315734. Andreas Deutsch is a member of the DFG Research Center for Regenerative Therapies Dresden Cluster of Excellence and gratefully acknowledges support by the Center.

REFERENCES

[1] M. Nakatsu, C. Hughes, *Methods Enzymol.* **443**, 65 (2008.).

[2] P. Carmeliet, *Nat. Med.* **9**, 653 (2003).

[3] P. Carmeliet, *Nature* **438**, 932 (2005).

[4] P. Carmeliet, R. Jain, *Nature* **473**, 298 (2011).

[5] R. Adams, K. Alitalo, *Nature Rev. Mol. Cell Biol.* **8**, 464 (2007).

[6] M. Chaplain, S. McDougall, A. Anderson, *Annu. Rev. Biomed. Eng.* **8**, 233 (2006).

[7] J. Chappell, S. Taylor, N. Ferrara, V. Bautch, *Dev. Cell* **17**, 377 (2009).

[8] H. Gerhardt *et al.*, *J. Cell. Biol.* **161**, 1163 (2003).

[9] R. Hynes, *Nat. Med.* **8**, 918 (2002).

[10] C. Jackson, *Curr. Opin. Nephrol. Hypertens.* **11**, 295 (2002).

[11] M. Pepper, *J. Thromb. Haemost.* **1**, 346 (2001).

[12] H. Meinhardt, *Models of Biological Pattern Formation*, Academic Press, London 1982.

[13] R. Merks, E. Perryn, A. Shirinifard, J. Glazier, *PLoS Comput. Biol.* **4**, e1000163 (2008).

[14] S. Raab *et al.*, *J. Thromb. Haemost.* **91**, 595 (2004).

[15] C. Mente *et al.*, "Parameter Estimation with a Novel Gradient-based Optimization Method for Biological Lattice-gas Cellular Automaton Models", *J. Math. Biol.*, available online, 2010.

[16] A. Deutsch, S. Dormann, *Cellular Automaton Modeling of Biological Pattern Formation*, Birkhauser, Boston, 2005.

[17] U. Frisch, B. Hasslacher, Y. Pomeau, *Phys. Rev. Lett.* **56**, 1505 (1986).

[18] H. Hatzikirou, L. Brusch, A. Deutsch, *Acta Phys. Pol. B Proc. Suppl.* **3**, 399 (2010).

[19] H. Hatzikirou, A. Deutsch, *Curr. Top. Develop. Biol.* **81**, 401 (2008).

[20] M. Tektonidis *et al.*, *J. Theor. Biol.* **287**, 131 (2011).

[21] D. Wolf-Gladrow, *Lattice-gas Cellular Automata and Lattice Boltzmann Models: An Introduction*, Springer, New York 2001.

[22] S. Arima *et al.*, "Angiogenic Morphogenesis Driven by Dynamic and Heterogeneous Collective Endothelial Cell Movement", *Development*, available online, 2011.

[23] P. Friedl, D. Gilmour, *Nature Rev. Mol. Cell Biol.* **10**, 445 (2009).

[24] S. Beikasim, M. Shridhar, M. Ahmadi, *Pattern Recognit.* **24**, 1117 (1991).

[25] Y. Bentoutou *et al.*, *Pattern Recognit.* **35**, 2853 (2002).

[26] J. Flusser, T. Suk, *Pattern Recognit.* **26**, 167 (1993).

[27] E. Dejana, E. Tournier-Lasserve, B.M. Weinstein, *Dev. Cell* **16**, 209 (2009).

[28] G. Breier, W. Risau, *Trends Cell Biol.* **6**, 454 (1996).

[29] E. Dejana, *Nature Rev. Mol. Cell Biol.* **5**, 261 (2004).

[30] N. Ferrara, T. Davis-Smyth, *Endocr. Rev.* **18**, 4 (1997).

[31] D. Senger, *PNAS* **94**, 13612 (1997).

[32] E. Unemori, N. Ferrara, E. Bauer, E.P. Amento, *J. Cell. Phys.* **153**, 557 (1992).